DESIGN AND OPTIMIZATION OF MIXED IONIC-ELECTRONIC CONDUCTIVE MATERIAL FOR USE IN SOLID OXIDE FUEL CELL UTILIZING CARBON NANOTUBES

by

SHIUAN-DUO CHIANG

Presented to the Faculty of the Graduate School of

The University of Texas at Arlington in Partial Fulfillment

of the Requirements

for the Degree of

MASTER OF SCIENCE IN MECHANICAL ENGINEERING

THE UNIVERSITY OF TEXAS AT ARLINGTON

May 2018

Acknowledgements

I would like to express my gratitude toward my supervising professor, Dr. Leila Ladani, for providing an opportunity to work with her. Dr. Ladani's constant guidance, patience and sharing of the knowledge throughout the research has inspired me to carry out the research work.

I am very grateful for Dr. Kenneth Reifsnider and Dr. Efstathios I. Meletis for serving as my committee member. Their input and suggestions have been very valuable for the completion of the research.

I would like to thank Shimadzu Institute Nanotechnology Research Center at the University of Texas at Arlington and especially Mr. Dennis Bueno, whom I had multiple occasions to work with. I want to thank him for his patience and technological support.

I would like to thank my lab mates and friends for being supportive and for their technical input.

Finally, I want to thank my family for their support and care.

April 12, 2018

Abstract

DESIGN AND OPTIMIZATION OF MIXED IONIC-ELECTRONIC CONDUCTIVE MATERIAL FOR USE IN SOLID OXIDE FUEL CELL UTILIZING CARBON NANOTUBES

SHIUAN-DUO CHIANG, MS

The University of Texas at Arlington, 2018

Supervising Professor: Leila Ladani

Triple phase boundary (TPB) is considered to be an important limiting factor of the fuel cell performance. Triple phase boundary is a geometrical line where the ionic, electronic and gaseous fuel phase of the fuel cell comes in contact. Electrochemical reactions of the fuel cell occur at the TPB sites. The TPB length greatly impacts the efficiency of the fuel cells. Carbon nanotubes have recently been shown to enhance oxygen reduction reaction (ORR) of the fuel cell and transfer electrons with its conductive properties. CNT also provides porosity in the electrode and could facilitate mass transport. CNT allows for oxygen and gas to permeate inside it to reach reaction sites.

This research theorizes a new model for the electrode material. This model utilizes CNT as the electronic phase and YSZ as the ionic phase. The two phases are mixed together to form a new kind of mixed ionic-electronic conductive (MIEC) material. MIEC allows for the electrode to be electronic and ionic conductive. MIEC allows for a denser TPB site throughout the electrode when compared to the traditional electrode. In traditional electrode TPB sites are only present at the interface of electrode and electrolyte.

A mathematical model is developed for this new material to calculate volumetric TPB length using geometrical values of the electrode. Different parameters are taken into account such as porosity, particle radius, CNT diameter, contact ratio of two phases, the distance between ionic particles and distance between CNT and particle. Graphs are produced to get a better understanding of the trends of TPB length when different parameters are altered.

Table of Contents

List of Illustrations

List of Symbols

a	semi-major axis
b	semi-minor axis
r	radius of cylinder
R	radius of sphere
c	distance from the axis of cylinder to center of sphere
CG	contact geometry
p	ellipse circumference
K	percent particle in contact with CNTs
ϕ	gas phase porosity
δ	CNT volume fraction
θ	Heaviside step function
Np	number of particles
Ltpb	Triple Phase Boundary length
vLtpb	Volumetric Triple Phase Boundary length
Vt	total volume of the electrode
Vti	total volume of the ionic phase particle
Vtl	total volume loss

Vlcs	total volume loss of the cylinder-sphere
Vlss	total volume loss sphere-sphere
d	distance between two intersecting spheres
r_1	intersecting sphere 1
r_2	intersecting sphere 2

Chapter 1. Introduction

What are Fuel Cells?

The challenge of this age is finding a cleaner and sustainable source of energy due to the world getting more conscious about environmental-friendly energy resources. As the technology advances more attention are being put on fuel cells by engineers and scientists. Fuel cell is a way to convert chemical energy of fuel gas into electrical energy. The combination of high efficiency with a direct conversion of energy and nonpolluting emissions of byproducts gives fuel cell a strong environmental advantage over traditional ways of generating power.

Fuel cell is a device that takes fuel as an input and produces electricity as output through electrochemical reaction [1]. As fuel is continuously being supplied into the fuel cell it will continue to produce electricity. This is the difference between fuel cells and battery. The battery depletes after a period of time when all stored chemical energy is used up and needs to be recharged, unlike the fuel cell. Heat engine also uses fuel to produce energy, but it works by combustion of fuel. Fuel cells do not require this intermediate step, which lowers the efficiency of the engine.

Fuel cell consists of electrodes and electrolytes. Electrode functions as a medium to bring about reaction between the reactant and the electrolyte. Electrode itself cannot be corroded by the fuel or oxidized by the reaction. There are two types of electrode present in a fuel cell, anode and cathode. At the anode side a catalyst oxidizes the fuel, commonly hydrogen, this allows electrons to be freed. The electrons travel out the anode to the circuit to create electricity. The hydrogen ions produced by the anode travel through the electrolyte to the cathode side. Oxygen on the cathode side is reduced into

oxide species. The ions are met with electrons from the circuit and react with oxide to form water.

Solid Oxide Fuel Cells

A particular kind of fuel cell that is Solid Oxide Fuel Cell (SOFC) carries great potential in providing cleaner energy. SOFC was only made possible today when Nerst invented the first solid oxide electrolyte in 1899 [2]. He made connection with the results of liquid electrolytes. It was until 1930 that Baur and Preis were able to successfully demonstrate a working solid oxide fuel cell using yttria-stabilised zirconia (YSZ) electrolyte at a temperature up to 1000^{o}C [3]. Since then more research has been conducted on SOFC that enable efficient and low-temperature SOFC to be produced.

As the name suggests solid oxide fuel cell is characterized by the solid-state electrolyte, comparing to usual fuel cells that utilize liquid electrolyte. Electrolyte functions as an ionic conductor that allows oxygen ions to migrate through the electrolyte film to retain charge balance. Like all other kinds of fuel cell electrodes are also key components of SOFC. Cathode which oxygen is reduced to oxygen ions passes through the electrolyte to anode. At anode oxygen ions react with the fuel, which is generally hydrogen, creating water and carbon dioxide. The chemical reaction of creating water gives out electrons, which flows out of the anode through the circuit and creates electrical power if there is an electrical connection between the anode and cathode. The components create what is called a “cell”.

To get a greater power output multiple cells have to be stacked together and joined with interconnect. There are several kinds of stack design of solid oxide fuel cells. The most common ones are tubular and planar design. Tubular design stacks meter long cells together to form an array of units. Operates with fuel flow on the outside of the

bundle of tubes and air on the inside. Planar configuration utilizes flat cell plates bonded together then stacked on top of each other to form a unit. Fuel and oxygen flow through the plate with different channel where each electrode is faced with its own reactant gases [4].

The main advantage of solid oxide fuel cell over other kinds of fuel cell is its high efficiency. They can have efficiency of over 60% and if the byproduct of heat is also harnessed the overall fuel to energy efficiency can be over 80% [5]. Another advantage of SOFC is the electrolyte is solid, which gives it greater flexibility in the cell structure. With normal aquatic electrolyte containment of the corrosive liquid must be taken into concern. The high temperature also gives SOFC a much wider choice of fuel [6]. Hydrocarbon could be internally reformed in the high temperature therefore natural gas, which is very available, could be used. The materials used in SOFC also do not contain any precious platinum electrocatalyst thus making its cost lower.

Solid oxide fuel cell does however come with its disadvantage. With many of the SOFC operating temperature going near 1000^{O}C materials has to withstand high temperature during its life cycle. This results in a higher system costs and degradation rate [7]. High operating temperature also means a slow startup and shutdown cycles. The focus of recent research on SOFC has been in reducing to an intermediate working temperature (650^{O}C~800 ^{O}C). At an even lower temperature (<650^{O}C) a vaster choice of material could be made. Lower cost of interconnects, seals, and insulation can be implanted. The main obstacle in lowering the operating temperature in SOFC is the electrolyte used. Yttria-stabilized zirconia (YSZ) is widely used as SOFC electrolyte due to its ion conductivity and stability [8]. The lower the temperature the lower the ionic conductivity of the YSZ electrolyte. Polarization loss at lower temperatures is associated

with electrolyte conduction and electrode reaction kinetics. It is the key issue that researchers have faced over the past.

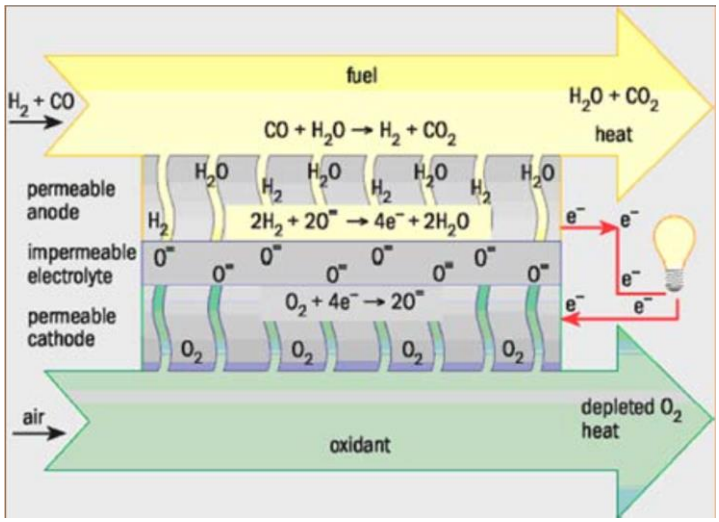

Figure 1-1. Scheme SOFC [9]

What materials are used in Solid Oxide Fuel Cells?

There are several properties to consider when it comes to the material consideration of the fuel cell.

- Stable within a reasonable lifetime.
- Conductivity: Ionic conductive for electrolyte and electric conductive for electrode.
- Chemically compatible between the components.
- Thermal expansion coefficient needs to match with the components to prevent fracture as SOFC could reach 1000^{O}C.
- Dense Electrolyte and Porous Electrode: Dense electrolyte to prevent fuel and air from mixing and flowing to the undesired compartment.

- High temperature: SOFC operates on temperatures as high as 1000^{O}C. The properties of the materials need to be able to withstand high temperature for a long duration of time.
- Fabricability: As most of the commonly used components are ceramic its fabricability with a certain desired configuration needs to be considered
- Cost of manufacturing [10]

The most commonly used material for electrolyte is YSZ A ceramic made by adding yttrium oxide (Y_2O_3) to zirconium dioxide (ZrO_2) to stabilize it. Zerconia changes crystal structures at high temperatures causing it to fracture. Adding yttria to zirconia will make Y^{3+} ions replace Zr^{4+} ions thus oxygen vacancies are generated.

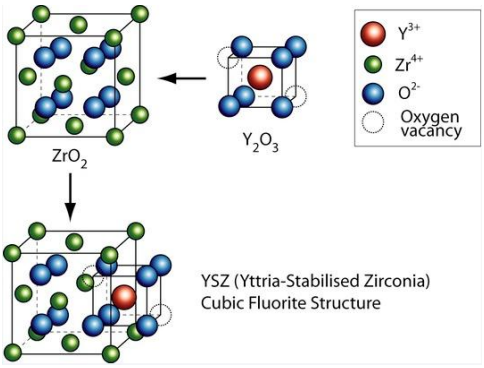

Figure 1-2. Structure of YSZ [11]

For cathode lanthanum manganites ($LaMnO_3$; LSM) is the most common material used in cathode due to its compatibility with YSZ. Strontium-doped lanthanum manganite ($LaSrMnO_3$) is created by doping Sr onto LSM. It increases the electron hole concentration and improves the electrical conductivity.

The most common anode material is Ni/YSZ cement. Due to the high catalytical activity of Ni H-H bonds could be broken. It's the most common material used in anode for its low cost, chemical stability, and thermal expansion coefficient (TEC).

History of CNT use in fuel cell

Carbon nanotubes (CNTs) poses many unique properties. There have been some attempts to use CNT in solid oxide fuel cell. The main difficulty to overcome is the operating temperature of SOFC is as high as 600~1000^{O}C. Comparing to thermal decomposition temperature of multiwall CNTs (MWCNTs) are at 420^{O}C in air. Additionally, MWCNTs will start to oxidize at 200 °C in an oxygen-rich environment [12].

Some researches use CNTs as an intermediate material to provide porous area for reaction to happen on electrodes. Multiwalled CNTs can be used for the synthesis of perovskite-type oxide nanoparticles. The samples were calcined at 700^{o}C, in order to obtain the crystalline phase. This kind of composite can be used for cathode for an intermediate temperature Solid oxide fuel cell [13]. Past research has also been done on electrophoretic deposition (EPD) of CNTs/ La0.6Sr0.4Co0.8Fe0.2O3d LSCF composite films on Ce0.9Gd0.1O1.95 (CGO) substrate. To get higher porosity they burn out the CNTs at 800^{o}C for one hour. Due to the high porosity the electrochemical performance and the kinetics of the oxygen reduction reaction of the LSFC cathode were enhanced [14].

Other kinds of attempts have been trying to improve the performance of the fuel cells by using CNTs to facilitate oxygen reduction reaction (ORR). ORR significantly affects the electrochemical performance of the fuel cells. One research uses vertically aligned nitrogen-containing carbon nanotubes (VA-NCNTs) to be implemented as the cathode of the fuel cell in order for oxygen reduction reaction (ORR) to take place [15]. The reasoning behind doping Nitrogen is to achieve a high positive charge density on carbon atoms adjacent to nitrogen atoms, which are electron-accepting. Research has also been done using poly (diallyldimethylammonium chloride) (PDDA). Using PDDA

researchers were able to withdraw electrons from carbon atoms on the nanotube to induce a positive charge that will facilitate the ORR activity. With the nonaligned CNT they disperse it in an aqueous solution of PDDA and with the vertically aligned CNT they spin-coated/infiltrating PDDA chains into the nanotube array [16].

Mixed Ionic-Electronic Conductors

Some of the key properties in defining materials used for fuel cells is the partial electronic and ionic conductivities. For solid oxide fuel cell electrolyte and electrochemical sensors should have a high oxygen ion conductivity, while electronic transport should be minimum. For SOFC electrodes and oxygen separation membranes both the ionic and electronic conductivity should be as high as possible [17]. Mixed ionic-electronic conductors (MIECs) are defined as materials that conduct both ions and electronic charge carriers. Having this kind of property, MIECs are commonly used as the electrode for their ability to conduct both ions and electrons. There are two types of MIECs, the first type consists of only one phase called true MIECs. An example would be $Ag_{2+\delta}S$, which conducts electrons and also silver ions, Ag^{+} [18]. $CeO_{2-\delta}$ is also a type of MIEC that conducts both oxygen ions and electronic charges [19]. Diffusion of oxygen is also observed in silver and as it being metallic it is obvious that it transfers free electrons [20]. Heterogeneous MIECs (H-MIECs) are mixtures of two phases, one phase conducts electrons and the other conducting ions. One common H-MIECs used in SOFC is Ni-YSZ. This composite material is used in anode for SOFC [21]. It is hard to find a true MIEC in some cases to apply to a certain condition, but by preparing a H-MIEC it is more feasible to mix material with two phases of ionic conducting phase and another electronic conducting phase.

There are some conditions to be fulfilled for ionic conduction to take place in solids. Three conditions must be fulfilled:[22]

- There should be an empty site in the forward direction, so that the ions can move forward
- Propagation from site to site is not impeded
- There should be a continues path from one side of the solid to the other

These sites can be formed by thermal excitation, change of stoichiometry and doping (introducing oxygen vacancies) [22].

Electronic conductivity occurs via conduction and valence bands or by thermally assisted hopping mechanism. It is generated in three ways deviation from stoichiometry

- Thermal excitation
- Deviation from stoichiometry
- Doping

Triple Phase Boundary

An important limiting factor of the fuel cell is triple phase boundary (TPB) [16]. There are three phases that come in contact of the triple phase boundary, which are the electrolyte, electrode and gaseous fuel. This boundary acts as the active region of the fuel cell which facilitates electrochemical reaction that produces power. As this is the limiting factor for fuel cell performance, increasing TPB density will also increase the reaction rate. The overall performance of fuel cell could be improved with increased TPB length. For traditional electrode and electrolyte materials, TPB will be found at the interface of the two objects. They each introduce a phase for TPB. For MIEC, two phases of materials are found within one volume of the electrode. The microparticle inside MIEC creates TPB within the electrode, not just on the interface. This extends TPB from a two-dimensional area to a three-dimensional volume.

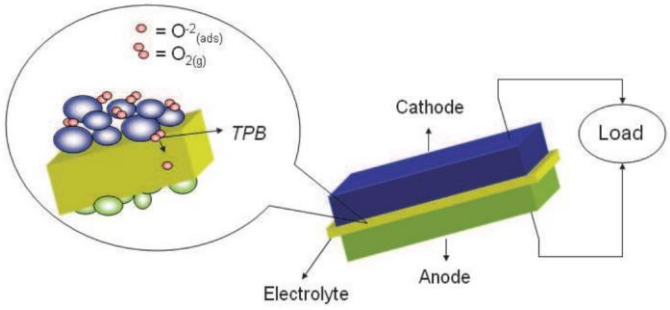

Figure 1-3. Triple phase boundary [23]

Objectives of thesis

There are many researches done on CNTs because of the potential of this material that possesses many interesting properties. Nevertheless, not a lot of research has been done on the possibility of it being complementary of solid oxide fuel cells. This thesis hopes to fill in the gap between these two distinct fields of research and considers the effect of CNT on the ceramic membrane of solid oxide fuel cells. A new model is presented and TPB length is calculated to evaluate this new theorized material. Through this research, a better understanding of the interaction of the CNT and fuel cell will be investigated.

Research plan and progress

Triple phase boundary will be analyzed in this research. Models for the structure of CNTs will be used to calculate the possible increase of the triple boundary phase length. With geometrically well-defined CNTs grown on the YSZ complexity of analyzing the triple phase boundary can be further reduced. A model will have to be developed by considering the geometric volume of the MWCNTs by its layers of walls and its radius. The geometry of the MWCNTs could be determined by scanning ion microscopy. By calculating the triple phase boundary if there is an increase in the length it will be confirmed as triple phase boundary is closely tied to the efficiency of the fuel cell and how the oxygen reduction reaction will occur.

At the same time of this research some preliminary experiments had been conducted. For us to be sure of the recipe for CNT growth trial runs have to be first conducted. Silicon wafers will be treated with thermal oxidation to grow SiO_2 on both sides of the wafer. Then using E-Beam thermal evaporation Ni is then deposited on both

sides of the wafer on the thickness of ~4nm. The wafer is then diced into 2by2 cm^2 squares for further CVD process. After successful runs of growing CNT parameters are then made sure of. For future experiments, we need to grow CNT on both sides of the silicon chip. Being sure of all the parameters of tests, we can then grow CNT on the actual ceramics. The processed ceramics is then sent for testing properties for ionic conduction.

Chapter 2. Defining the Model

The model defined here is a theoretical improvement based on the current materials and configurations used for Solid Oxide Fuel Cells (SOFC). A new design of Mixed Ionic-Electronic Conductor (MIEC) is proposed. This new design utilizes carbon nanotubes (CNT) as the electronic phase in the complement of spherical ionic grain particle. Triple Boundary Phase (TPB) length is calculated to theorize how this configuration would perform.

This model is characterized by having CNT radius (R) and ionic phase particle radius (r). It is assumed that the electronic phase CNT is to be treated as a cylinder and the ionic phase YSZ as a sphere. Assume the cylinder and the sphere overlap and creates an intersecting volume. Around the part that intersects is the line of contact, that line will be the area where the three phases, electronic, ionic and gaseous fuel will come in contact together and is defined as the triple phase boundary (TPB).

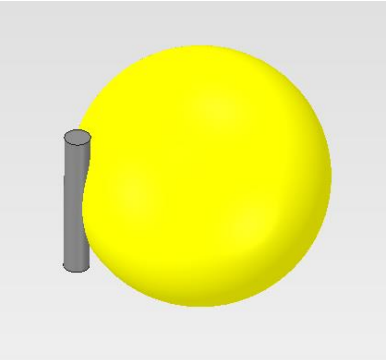

Figure 2-1. Intersecting CNT and YSZ particle

Chapter 3. Mathematical Model of TPB

Equation for Triple Phase Boundary

The main objective of the mathematical model is to calculate the volume specific Triple Phase Boundary length of the mixed ionic-electronic conductor. We start the calculation by defining the ultimate formula that we will be calculating for the TPB length

$$L_{tpb} = Np \times K \times CG \times \emptyset \quad (1)$$

L_{tpb} stands for the length of the triple boundary phase for the whole material. Np is the number of particles for the ionic state and K stands for the contact ratio of the electronic phase per ionic phase particle. Np multiple by K gives the total site of contact with the ionic phase and electronic phase. This in term tells us how many sites that we will have triple phase boundary in the composite ceramic. CG stands for contact geometry, it is the length of contact with electronic phase and ionic phase per site. By multiplying this parameter, it gives the total length of contact of the electronic phase and ionic phase. ϕ is the gas porosity. It defines the fractional volume of gas of the total volume considered. For electrochemical reaction on the Triple Phase Boundary sites to occur the total length of contact of the electronic phase and ionic phase must also be exposed to gaseous fuel. The multiplication of the length of contact of the electronic phase and ionic phase with the gas phase porosity gives the total length of the triple phase boundary in the electrode.

This will be the ultimate equation that gives the total triple phase boundary length of the whole electrode. Dividing both sides of the equation will give the vL_{tpb}, which is the

volume specific triple phase boundary length. This parameter is more intuitive to evaluate the relationship between volume of electrode and TPB length that it provides.

Contact Geometry of CNT Ionic Phase Particle

To calculate the triple phase boundary length per site we start by assuming CNT to be a cylinder and the ionic phase particle to be a sphere. It is also assumed that the cylinder and the sphere overlaps and there will be a volume of the intersecting solid. The line where the cylinder and the sphere meet will be the place where electronic phase and ionic phase meets and electrochemical reaction of the electrode would happen. If the line that circles around the intersection is flattened out, an ellipse will form and the circumference of the ellipse could be calculated using the geometries of the intersecting sphere and cylinder.

Here *a* is the semi-major axis and *b* is the semi-minor axis. The circumference *p* of the ellipse could be calculated through the two parameters with approximation formulas.

$$p \approx \pi \left[3(a+b) - \sqrt{(3a+b)(a+3b)} \right] \tag{2}$$

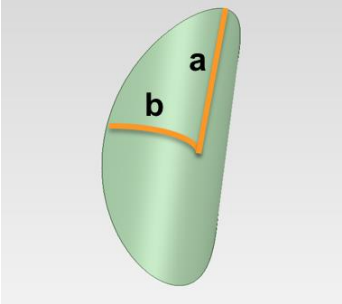

Figure 3-1. Intersecting volume of a sphere and cylinder

Calculation of parameter *a*

To get the semi-major axis *a* several geometric values are considered. The radius of the cylinder that represents the CNT is *r*. The radius of the sphere that is the ionic phase particle is *R*. *c* stands for the distance of the axis of the cylinder to the center of the sphere. If we deduct the distance of the axis of the cylinder to the center of the sphere with the radius of the cylinder we have the distance from the center of the sphere to the edge of the cylinder. The value forms a triangle with semi-major axis *a* and radius of the sphere. The expression for *a* can be calculated through basic Pythagorean theorem.

$$a = \sqrt{R^2 - (c - r)^2} \tag{3}$$

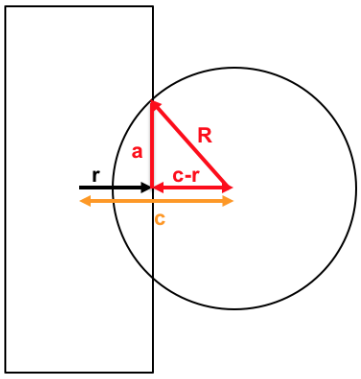

Figure 3-2. Side view of cylinder and sphere

a: semi-major axis

r: radius of cylinder

R: radius of sphere

c: distance from the axis of cylinder to center of sphere

Calculation of parameter *b*

For calculation of semi-minor axis *b*, the same parameters are used for the radius of the cylinder, radius of ionic phase sphere and distance of cylinder axis to sphere center. To calculate *b,* the geometry is viewed from a top-down angle. The curve of cylinder that starts from the intersection of the cylinder-sphere and ends where the line *c* intersects is *b.* It is a part of the wall of the cylinder. To acquire the curve length the degree of curvature of the curve *b* is to be calculated. The three parameters: radius of the cylinder, radius of ionic phase sphere and distance of cylinder axis to sphere center will form a triangle. Angle between side r and c can be calculated by The Law of Cosines with the three-known side (sss problem).

$$\theta = \cos^{-1}\left(\frac{r^2 + c^2 - R^2}{2rc}\right) \tag{4}$$

With the known degree of curvature, the length of *b*, which is a part of the circumference of the CNT can be calculated.

$$b = 2\pi r \times \frac{\theta}{360}° \tag{5}$$

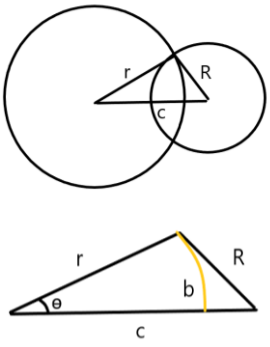

Figure 3-3. Top-down view of cylinder and sphere

With the semi-major axis and semi-minor axis calculated the circumference of the ellipse can be calculated through approximation formulas.

Number of ionic phase particles

For the porous electrode, we have Np as the number of ionic phase particle in the total volume. Let V_t be the total volume of the electrode under consideration and V_{ti} be the total volume of the ionic phase particle, then

$$V_{ti} = (1 - \emptyset)(1 - \delta)V_t \tag{6}$$

where ϕ is the gas and δ is the volume fraction of the ionic phase particle over the whole solid.

The total volume of the ionic phase particle could also be presented as a function of the number of ionic phase particle Np.

$$V_{ti} = Np\frac{4}{3}\pi R^3 - V_t \tag{7}$$

r stands for the radius of the ionic phase particle, which is considered as a sphere. The volume of the sphere multiply by the total number of particle gives the total volume. V_{tl} is the total volume loss of the ionic phase particle. These ionic phase particles, like YSZ overlaps each other thus creating spaces that are intersecting. The intersecting volume must be deducted to get a more accurate volume of the ionic phase.

Combine the two equations,

$$(1 - \emptyset)(1 - \delta)V_t = Np\frac{4}{3}\pi R^3 - V_t \tag{8}$$

Express the equation for number of ionic particles Np,

$$Np = \frac{(1-\emptyset)(1-\delta)V_t + V_{tl}}{\frac{4}{3}\pi R^3} \tag{9}$$

Total Volume Loss

With the overlapping portions of the ionic phase particle there are two types of overlap to take into account. The sphere attaching to the cylinder creates volume loss on the sphere. The ionic phase particles itself are intersecting with each other.

Intersecting volume of cylinder and sphere

François and Claude developed the analytical expression for the volume of intersection of a sphere with a cylinder. The volume of intersection would be a function of the distance between the axis of the cylinder and the center of the sphere, the radius of the cylinder and the radius of the sphere [24].

Consider the volume defined by the intersection of the cylinder of radius r with the sphere of radius R [24]. Here *b* is the distance of the cylinder axis to the center of the sphere.

$$V(r,R,b) = 2 \int\limits_{(x-b)^2+y^2 \le r^2} \int\limits_{x^2+y^2 \le R^2} \sqrt{R^2 - x^2 - y^2}\, dx\, dy \tag{10}$$

There are several different configurations to consider with the relative placement of the cylinder and sphere and also the radius.

If the volume is at zero impact parameter (*b=0).*

$$V(r,R,0) = \int_0^r 2\pi x \left(2\sqrt{R^2 - x^2}\right) dx = \frac{4\pi}{3}R^3 - \frac{4\pi}{3}(R^2 - r^2)^{\frac{3}{2}},\ R \ge r \tag{11}$$

$$V(r,R,0) = \frac{4\pi}{3}R^3, \qquad R < r \tag{12}$$

If $r > R+b$, the volume of the cylinder fully consumes the sphere and the volume of intersection will simply be the volume of the sphere.

Cases of expression for the volume of intersection of a sphere with a cylinder where b does not equal to zero are as follows,

We could first think of b and r to be a fixed parameter and depending on the length of the radius of the sphere, it will intersect the cylinder differently in each case.

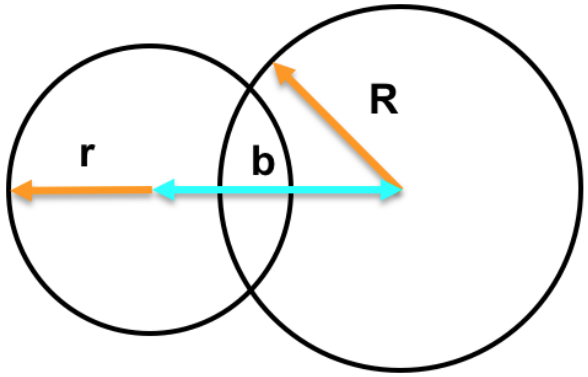

Figure 3-4. Cylinder sphere intersecting radius

The first case is where the sphere is larger than the distance b plus radius of the cylinder. The sphere completely crosses over to the other side of the cylinder.

$$V(r,R,b) = \frac{4\pi}{3}R^3\theta(r-b) + \frac{4}{3\sqrt{A-C}}\left[\Pi(k,-\alpha^2)\frac{A^2 s}{C} - K(k)\left(As - \frac{(A-B)(A-C)}{3}\right) - E(k)(A-C)\left(s + \frac{4A-2B-2C}{3}\right)\right], \quad R > b + r \qquad (13)$$

The second case is where the sphere is shorter than the distance b plus radius of cylinder. The sphere intersects the cylinder somewhere in between and does not completely crosses over to the other side of the cylinder.

$$V(r,R,b) = \frac{4\pi}{3}R^3\theta(r-b)$$

$$+\frac{4/3}{\sqrt{A-C}}\left[\Pi(k,-\alpha^2)\frac{B^2 s}{C}\right.$$

$$-K(k)\left(s(A-2B)+(A+B)\frac{3B-C-2A}{3}\right)$$

$$\left.-E(k)(A-C)\left(-s+\frac{2A-2C-4B}{3}\right)\right], \qquad R<b+r \qquad (14)$$

The third case is where the sphere is equaled to the distance b plus radius of the cylinder. The edge of the sphere intersects the cylinder on the other side and.

$$V(r,R,b) = \frac{4\pi}{3}R^3\theta(r-b)$$

$$+\frac{4}{3}R^3\arctan\left(\frac{2\sqrt{br}}{b-r}\right)-\frac{4}{3}\sqrt{A-C}-\left(s+\frac{2}{3}(A-C)\right), \qquad R=b+r \qquad (15)$$

θ denotes the Heaviside step function and the other functions are as follows,

$$K(k) = \int_0^1 \frac{dz}{\sqrt{1-z^2}\sqrt{1-k^2z^2}}$$

$$Z(k) = \int_0^1 \frac{dz\sqrt{1-z^2}}{\sqrt{1-k^2z^2}}$$

$$\Pi(k,-\alpha^2) = \int_0^1 \frac{dz}{(1-\alpha^2z^2)\sqrt{1-z^2}\sqrt{1-k^2z^2}}$$

Properties of the above functions and quantities defined,

$$A = \max(R^2, (b+r)^2),$$

$$B = \min(R^2, (b+r)^2),$$

$$C = (\mathrm{b} - \mathrm{r})^2,$$

$$k^2 = \frac{B-C}{A-C},$$

$$-\alpha^2 = \frac{B-C}{A-C},$$

$$s = (b+r)(b-r),$$

For the purpose of this research a particular case of $R < b+r$ is chosen. The radius of the sphere is shorter than the distance of the cylinder axis to the center of sphere plus the radius of the cylinder. This is due to the fact that an ionic phase particle should be touching the carbon nanotubes, but not completely overlapping the CNT and covering it. The second case is chosen for this purpose. V_{lcs} is defined to be the volume loss of cylinder and sphere.

Intersecting Volume of sphere-sphere

The mixed ionic-electronic electrode consists of YZS ionic phase particles. The ionic phase solid phase is made up of spherical particles. These particles form a porous electrode and individual particle are intersecting each other. Consider two spheres with radius r_1 and r_2. The intersecting volume of the spheres is calculated by summing the two spherical caps.

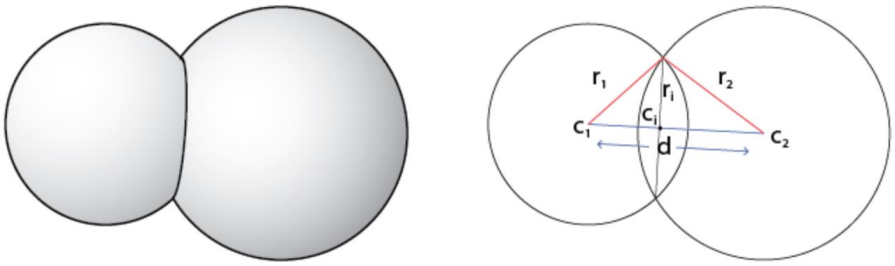

Figure 3-5. Intersecting sphere [25]

The equation for calculating spherical caps of height *h* and sphere radius *R*.

$$V(h,R) = \frac{1}{3}\pi h^2(3R-h) \tag{16}$$

Let r_1 and r_2 be the radius of the two spheres. Summing the two spherical caps will equal to the volume loss of the two spheres.

$$V_{lss} = V(h_1,r_1) + V(h_2,r_2)$$

$$= \frac{\pi(r_1+r_2-d^2)(d^2+2dr_1-3{r_2}^2+2dr_1+6r_1r_2-3{r_1}^2)}{12d} \tag{17}$$

Since all that is considered is the same type of ionic particle [26]. r_1=r_2 so,

$$V_{lss} = \frac{1}{12}\pi(4R+d)(2R-d)^2 \tag{18}$$

V_{lss} is defined as the volume loss of the ionic phase sphere with the same radius.

Total Number of particles

The total volume loss of the whole electrode will be acquired by summing the volume loss of cylinder and sphere and the volume loss of sphere and sphere.

$$V_{tl} = Np \times K \times V_{lcs} + Np \times V_{lss} \tag{19}$$

Then substitute this equation into the equation of total volume of ionic phase.

$$(1 - \emptyset)(1 - \delta)V_t = Np\frac{4}{3}\pi r^3 - V_{tl} \tag{20}$$

we can get,

$$(1 - \emptyset)(1 - \delta)V_t = Np\frac{4}{3}\pi R^3 - Np \times K \times V_{lcs} + Np \times V_{lss} \tag{21}$$

Express the equation for number of ionic particles Np,

$$Np = \frac{(1 - \emptyset)(1 - \delta)V_t}{\frac{4}{3}\pi R^3 - K \times V_{lcs} - V_{lss}} \tag{22}$$

TPB length per unit volume

The expression for the number of ionic particles and the contact geometry is known through the previous expression. Insert the equations into the equation for triple phase boundary length

$$L_{tpb} = Np \times K \times CG \times \emptyset$$

then it is concluded to be,

$$L_{tpb} = \frac{(1 - \emptyset)(1 - \delta)V_t}{\frac{4}{3}\pi R^3 - K \times V_{lcs} - V_{lss}} \times K \times CG \times \emptyset \tag{23}$$

It is also of interest to know the TPB length per unit volume of electrode, so for the equation divide both sides by V_t.

$$\upsilon L_{tpb} = \frac{(1-\emptyset)(1-\delta)}{\frac{4}{3}\pi R^3 - K \times V_{lcs} - V_{lss}} \times K \times CG \times \emptyset \qquad (24)$$

K stands for the contact ratio of the electronic phase per ionic phase particle. CG stands for contact geometry and is given by the equation for the circumference of the ellipse

$$p \approx \pi[3(a+b) - \sqrt{(3a+b)(a+3b)}]$$

With semi-major axis *a* and semi-minor axis *b*

$$a = \sqrt{R^2 - (c-r)^2}$$

$$b = 2\pi r \times \theta/360°$$

For the last part, ∅ is the gas phase porosity of the electrode. This gives the total length of the boundary with ionic phase and electronic phase. The boundary only becomes a three-phase boundary if the intersecting CNT and ionic particle is associated with a pore space, therefore it is multiplied by gas phase porosity at the end of the equation.

Chapter 4. Results and Discussion

A geometric based approach is used to calculate the triple phase boundary per unit volume of the electrode of mixed ionic-electronic conductors of solid oxide fuel cell. The model is based on the geometric properties of CNT and YSZ particles acting as the electronic phase and ionic phase. CNT is assumed to be a cylindrical shape and YSZ to be spherical. The ionic phase particle is assumed to be the same size and also assumed to be intersecting each other and also intersecting the CNT. By graphing the following equation with variable porosity while other parameters are fixed,

$$vL_{tpb} = \frac{(1-\emptyset)(1-\delta)}{\frac{4}{3}\pi R^3 - K \times V_{lcs} - V_{lss}} \times K \times CG \times \emptyset$$

we get the following Figure 4-1.

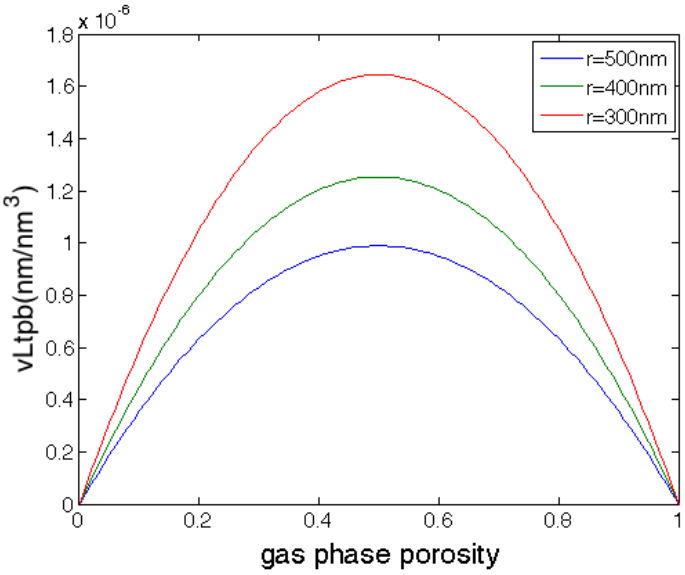

Figure 4-1. Volumetric TPB length as a function of gas phase porosity for different ionic particle size

As predicted by the equation for triple phase boundary for unit volume the maximum vLtpb is observed at 50% porosity. Maximum vLtpb at 50% porosity is observed regardless of grain sizes. For fixed gas phase porosity, as the grain decreases the vLtpb increases.

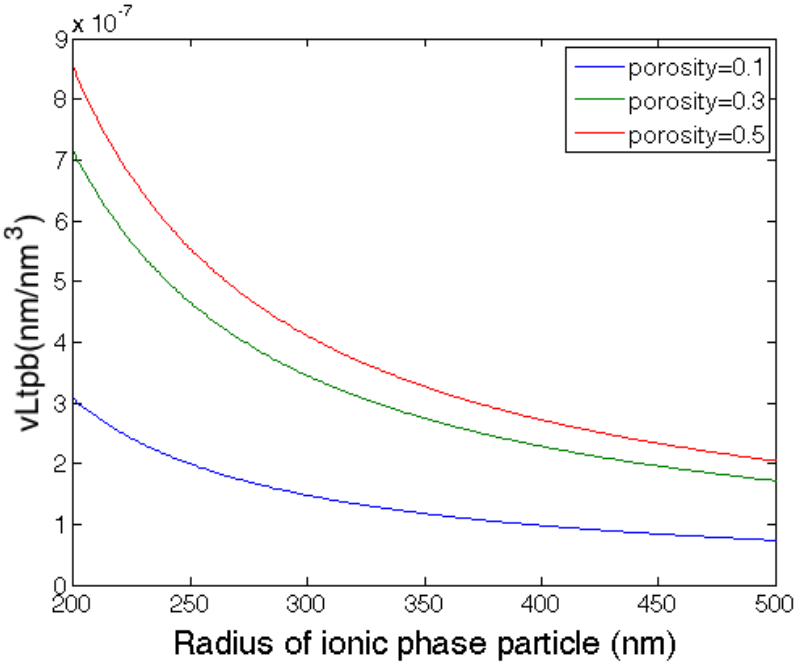

Figure 4-2. vLtpb length as a function of radius of ionic phase particle with different porosity

For Figure 4-2, it displays the volumetric TPB length for various porosity with the function of ionic phase grain size. Similar to Figure 4-1., vLtpb increases as the grain decreases and with increasing porosity. It also should be noted that increasing the porosity after 50% will result in a decrease of vLtpb.

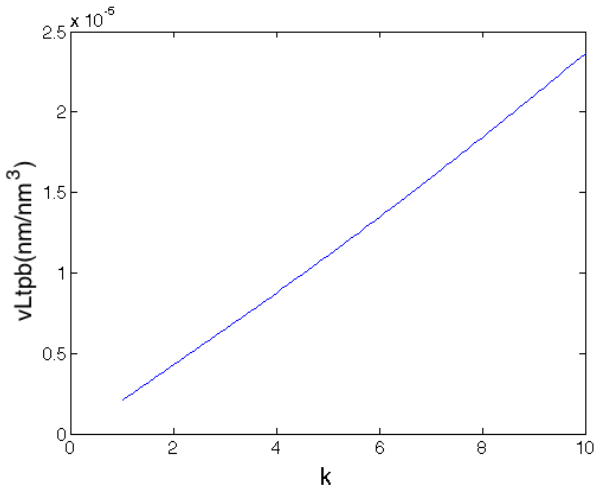

Figure 4-3. vLtpb as a function of contact ratio K

Quite intuitively from the equation the vLtpb increase linearly with contact ratio K increasing. Figure 4-4. plots the influence of distance between the ionic phase particle and CNT on volume specific triple phase boundary length. As the distance between the ionic phase particle and CNT widens, there is a decrease in vLtpb. From a geometric standpoint, the contact geometry of the ionic phase particle and CNT decreases as they are pulled apart and thus the shorter vLtpb length.

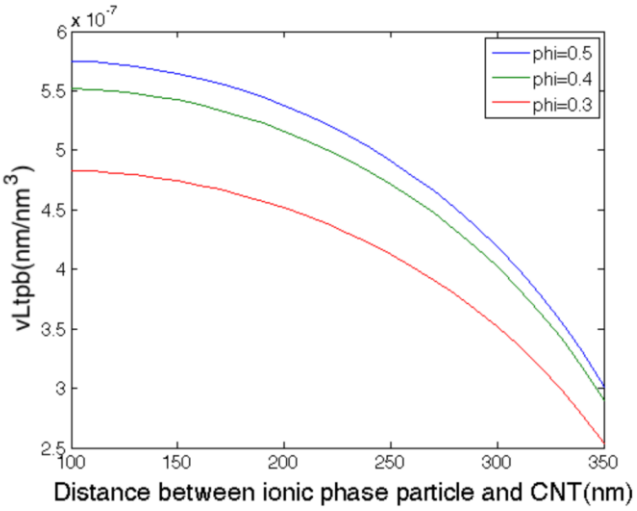

Figure 4-4. vLtpb as a function of distance between ionic phase and electronic phase

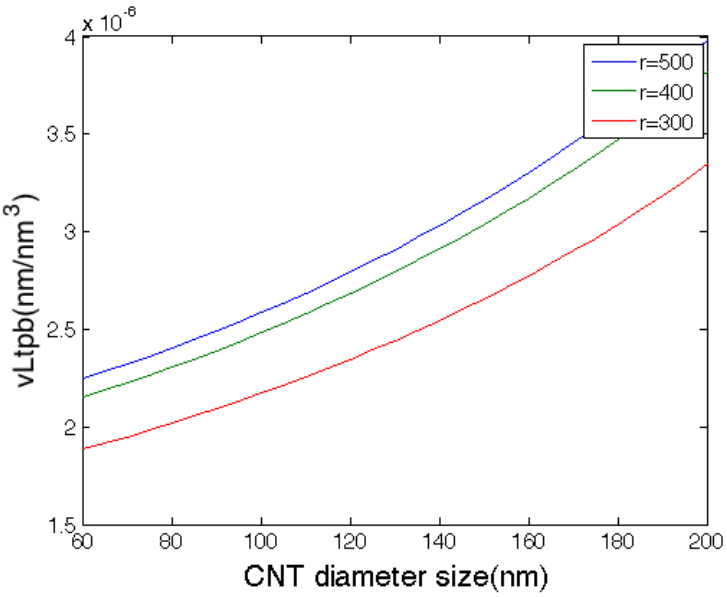

Figure 4-5. vLtpb as a function of CNT diameter with varied ionic particle size

Figure 4-5. plots the influence of CNT diameter size on volume specific triple phase boundary length. Increasing the CNT diameter results in an overall increase in contact geometry and leads to TPB length being longer.

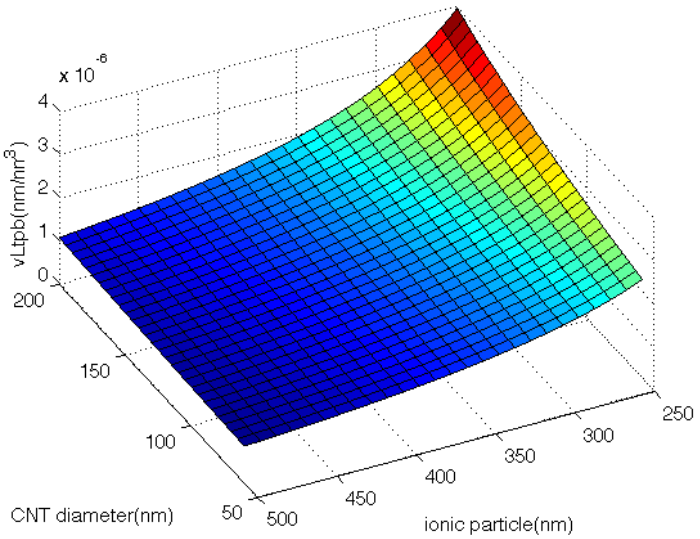

Figure 4-6. 3D plot of vLtpb as a function of CNT diameter and ionic particle radius

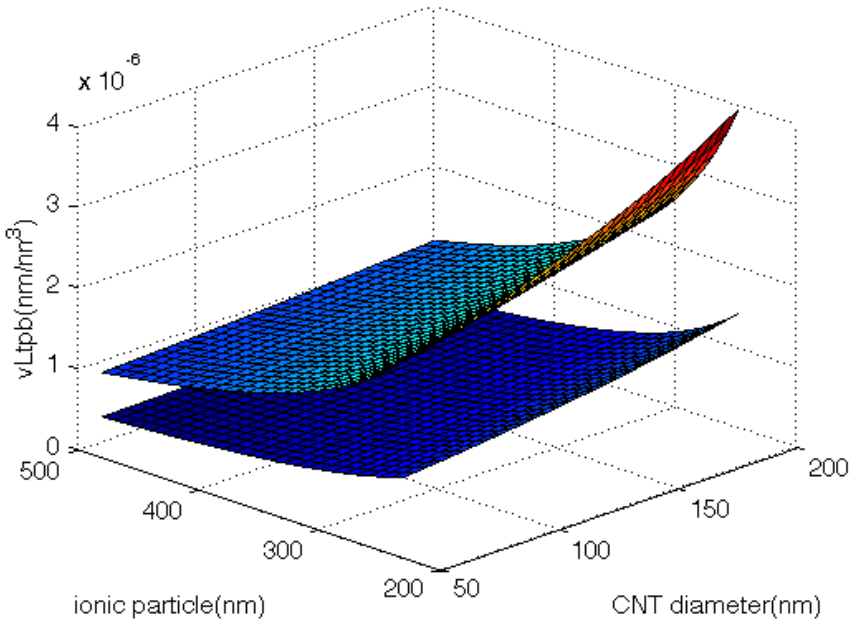

Figure 4-7. 3D plot of vLtpb as a function of CNT diameter and ionic particle radius with gas phase porosity of 0.5 as the upper layer and 0.1 as the lower layer

Figure 4-6. and Figure 4-7. is a 3D graph of the vLtpb as the z axis as a function of ionic phase particle size and CNT diameter size. Different layers are representing different gas phase porosity in the 3D graph. The results are similar to that of previous graphs. As ionic phase particle size decreases the vLtpb length increases and as the CNT diameter size increases the vLtpb length increases.

Validation Using Experimental and Literature Data

Mathematical approach is a simple and efficient way to estimate TPB length of a particular MIEC electrode. To compare the results with actual experiments we could look into some research that utilizes FIB-SEM to reconstruct models of the electrode microstructure. Wilson et al. used dual-beam focused ion beam-scanning electron microscopy to create a three-dimensional model of a Ni-YSZ cermet anode [26]. A series of 2D cross-sectional SEM image was collected while the electrode is milled layer by layer along the third axis by FIB. Surface of the electrode was first cut and polished. FIB was used to mill a trench into the surface. The electron beam could then be used to take image of the side of the trench from a 36° angle from normal to the wall. The FIB continued to mill the wall as the SEM image were acquired layer by layer. The scan rate of SEM is synchronized with the milling rate of FIB for high quality imaging.

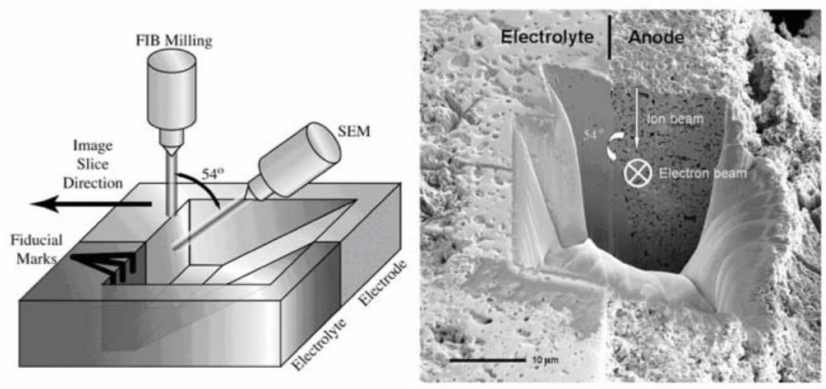

Figure 4-8. Schematic drawing of FIB-SEM, and SEM image of a FIB-etched region [26]

After image acquisition, it is important to align the images in order to make a 3D model. By using fiducial marks as reference researchers were able stack 82 consecutive image and the total volume analyzed was ~ 100 μm^3. Different pixels were assigned to different phases, Ni, YSZ or pore. Volume percentage of Ni, YSZ and pores from the 3D

image were 25.9%, 54.6% and 19.5%. Subsequent analysis found that the volume specific TPB length is 4.28×10^{12} m/m^3. Comparing similar research approach for using FIB-SEM to calculate TPB length, researches from Kishimoto et al. have found the volume specific TPB length of Ni-YSZ to be 2.49×10^{12} m/m^3 [27]. Shikazono et al. have the volume specific TPB length at 2.556×10^{12} m/m^3 [28]. These researches all implement FIB-SEM to create 3D model to calculate TPB length of different Ni-YSZ block but have coherent results with magnitude. In terms of magnitude it is close to what the calculations here have shown for TPB length analysis in this research. Although what is calculated in this research is a new kind of MIEC, CNT-YSZ, it is still important to know and compare what the TPB would be like for typical materials used for SOFC electrode using existing experimental data from various researches.

Chapter 5. Conclusion

Research had been done in the past calculating the triple phase boundary length of solid oxide fuel cells. Most researches have focused on the spherical geometric shape of the ionic phase particle. A new model is proposed here and analyzed. CNT and YSZ act as a two-phase conductor for this mixed ionic-electronic material. This model utilizes geometric properties of CNT and YSZ to derive mathematical equations calculated for volumetric TPB length (vL_{tpb}) for the new composite electrode. In terms of magnitude, the resulting TPB length is close to that of Wilson et al. [27]. The study used ion-beam scanning electron microscopy to estimate the volume-specific TPB length to be 4.28×10^{12} m/m^3. Graphs were plotted to understand how this type of model would change the TPB length under different parameters. It is observed that at 50% porosity, there will be max vL_{tpb} for certain ionic phase particle size. Volumetric TPB length increases as the ionic phase particle size decreases and CNT diameter size increase. Volumetric TPB length increases linearly with linear increase of contact ratio with CNT and ionic phase particle. As the distance between the CNT and ionic phase particle increase the TPB length per site decreases, thus overall volumetric TPB length also decreases.

Future research could be looking into the fabrication of CNT-YSZ composite and using FIB-SEM to create a 3D model to calculate TPB length. Compare TPB length results with the theoretical model to further optimize the mathematical equations.

Chapter 6. Future Work

CNT Fabrication

Some preliminary fabrication has been done to fabricate CNT. The substrate for growing CNT is fabricated at Shimadzu Institute Nanotechnology Research Center at the University of Texas at Arlington. The process of growing CNT using CVD machine are done at University of Northern Texas Physics Department.

The simplified steps of MWCNT growth process experimented are as follows:

1. Substrate [Si/SiO2(300nm)/Ni(5nm)] 5nm Ni is coated both sides
2. Vacuum the CVD system at 10-3 [millibar or millitorr]
3. Pretreatment (temperature was ramped to 700 ^{O}C)
4. H_2 gas at 150 sccm for 15 min and reduced to 50 sccm
5. C_2H_2 at 50 sccm for 20 min (mixture of 50 sccm H2 and 50 sccm C_2H_2)

We were able to get some CNT on the surface of the substrate although it is an uneven distribution of CNT patches. Further experiments have to be made to finalize recipe and process.

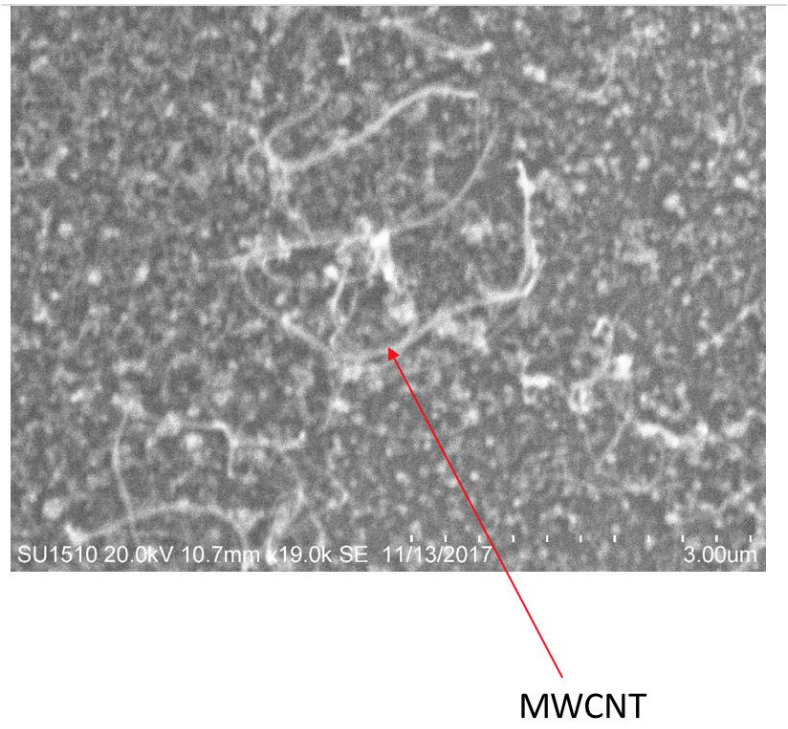

Figure 6-1. Image of MWCNT

Practicality of Fabricating YSZ-CNT composite

Calculations of TPB length for this type of MIEC has been theorized. To further explore the practicality of utilizing this material in existing fuel cells the fabrication must be taken into consideration. YSZ particle size typical ranges from 0.5-1.0 μm [30]. Other coarser YSZ powder has also been used and is reported to be around 1-4 μm [30][31][32]. On the electric phase we have CNTs that are typically around 30 nm, but studies of large diameter CNT have also been made. Some of the large diameter CNT could range from 50-150 nm [33]. Since we are using a two-phase MIEC, how to mix and

combine the two material is the main problem. We could look into some of the common material of fuel cell components and how they are fabricated.

For common YSZ ceramic YSZ powders are used as the raw material. These YSZ powders are usually made by spray drying method, liquid phase method and grinding method [34]. These powders are uniform and spherical shaped. With the YSZ powders, films are made by tape casting, tape calendaring and gel casting process [32]. The films can then be cut into the desired shape usually in disk. The samples are then sintered in a furnace. Sintering temperature is usually around 1000 to 1200 ^{O}C [35]. The starting temperature that YSZ begins to sinter depends on the grain size, the smaller the grain size the lower temperature it starts to sinter [32].

Ni-YSZ is a type of mixed phase ceramic that is commonly used in the anode for SOFC. This could be of reference for our new type of material. Ni-YSZ cermet has high electrochemical activity, chemical stability and compatibility with electrolyte materials. The fabrication of NiO-YSZ starts with forming a powder mixture. The NiO powder and YSZ powder is prepared and mixed in distilled water then ball milled to form a slurry [36]. For a gel casting method, the mixed slurry then goes through casting and gelation by pouring the slurry in a mold and heating in an oven. The resulting gel could then be cut into discs and dried [36]. Another type of method involves dried NiO-YSZ composite powders. These powders are compacted under uni-axial pressure to form a disc [37]. The compacted anode is then sintered for 1300^{O}C. This could be the substrate of anode supported electrolyte. The YSZ slurry can be dip-coated onto the anode to form electrolyte. The whole anode supported electrolyte can then be sintered at 1400^{O}C [37]. This yield a thin electrolyte film (<7μm) that have a lower ionic transport resistant.

(La0.8Sr0.2)0.97MnO3 (LSM) is a common material used for cathode for its high electrochemical activity for oxygen reduction and its compatibility for YSZ. In low-

temperature state, the oxygen ion conductivity is not up to standard and a mix of YSZ is needed for ionic phase transport. This extends the TPB from electrode and electrolyte boundary to inside the composite electrode. To prepare an LSM electrode several fabrication methods are available such as tape casting, screen printing and gel-casting [38][39]. Chemical vapor deposition (CVD) and electrochemical vapor deposition (EVD) is also used in some research, but a controlled atmosphere and sophisticated equipment increases the difficulty and cost of fabrication. In recent studies, spray pyrolysis is found to be an efficient way to deposit a thin layer of LSM on the surface of electrolyte [40]. Aerosol deposition is also found to be of great effectiveness of depositing LSM-YSZ powders on YSZ/NiO-YSZ substrate. This process has a high deposition rate with high adhesion strength and can be achieved at room temperature [41].

The possibility of fabricating YSZ-CNT composite electrode is the main issue when expanding the concept of this thesis into experimental situations. Recently, there are some researches that have fabricated YSZ-CNT composite successfully. There is a limited amount of research on this topic, but most of the fabrication of this type of material has been done using spark plasma sintering (SPS). Contrast to traditional sintering for YSZ, traditional sintering often results in a high thermal gradient that leads to cracks, change of shape and uneven microstructure evolution [42]. A way to prevent these poor qualities is to decrease the heating rate and cooling rate of the sintering process. Spark plasma sintering (SPS) is being researched for its crack -free samples and faster heating and cooling rates. SPS utilizes joule heating, it produces heat through passing the electric current through the conductor [43]. This kind of heat generation is internal compared to traditional sintering method which applies heat through an external source. Joule heating leads to a homogeneous thermal profile in the ceramic. By increasing SPS

temperatures researchers have found that the grain size increases and density of the ceramic also increase [44].

On recent reviews of researches done, there are still several difficulties if we are producing a CNT-YSZ composite. One of the difficulties would be to avoid damage to CNT during SPS. High temperature could break, oxidize or destruct crystal structures of the CNT. Bonding of the CNT and YSZ is also a point to consider when the two-phase needs to intersect for electrochemical reactions to occur. Interfacial compatibility and adhesion of CNT and YSZ with entanglement of CNT to ceramic particles will be an important factor. It is also important to achieve homogeneous distribution of the CNT throughout the ceramic. CNT tends to cluster together with Van der Waals forces. Density is tightly related to sintering temperature. To achieve certain density precision control of temperature and sintering time is of utmost importance [45].

For preparing the two-phase powders, CNT-YSZ were stirred and prepared using bath-tip sonication [46]. The slurries are then baked and cooled to room temperature. Then it is sintered using SPS machine with Ar atmosphere to prevent CNT degradation. Other researches prepared the CNT-YSZ powder by attrition milling with zirconia balls and the samples would then be processed through SPS [45]. Conventional method like hot pressing has also been researched. CNT and YSZ is mixed with a dispersant and binder. Mixed powders are then spray dried and hot pressed at $1300^{O}C$ for 30 minutes [47].

Researches have shown CNT-YSZ composites to have significant improvement of mechanical properties with enhanced toughness and resistance to cracking [46][45]. With CNT-YSZ composites being researched for its mechanical properties not much have been done regarding its ionic and electronic conductivity. TPB length, ionic and electronic conductivity would be of further interest related to this research. These properties could

be evaluated in the future and analyze how this material could perform in a fuel cell. How this type of fabrication method for YSZ-CNT suits our research purpose has to be further investigated.

3D Model Reconstruction of Microstructure and TPB length analysis

Mathematical model predicts TPB length in a perfect scenario with multiple assumptions made. Further assessment of TPB in an experimental setup could be used to compare theoretical calculations with modeled electrode. Most computer-assisted TPB estimation method has been using FIB or SEM to scan a composite electrode. The data is then used to generate a 3D reconstruction model of the porous electrode. Different phases are defined within the model and differentiated with color schemes. With the 3D model well defined the simulation can then calculate the TPB length for a certain cubic volume.

Reported by Holzer et al. FIB-SEM was used to reconstruct a 3D model of the electrode [48]. The pores are first filled with resin to create a flat cross-section for SEM 2D analysis. The sample is then grinded with SiC paper and polished. Finally, it is coated with a thin carbon layer with a few nanometers of thickness. FIB is used to produce a perfectly flat cross-section on the samples. These cross section is then scanned for SEM 2D imaging. The sequence for analyzing the whole sample is a slice and scan procedure. Multiple 2D images are then combined together to form a 3D-reconstruction of the sample. After sample preparation and imaging its necessary to do segmentation of different phases. Segmentation is done based on different grey scale. Materials will be separated by different grey scale values under SEM imaging. One problem presented by this method is that the boundary or the transition zone is a gradual change of grey scale

value. To avoid this problem, geometrical criteria is taken into account. The processed image results in a sharp intersection between two materials. [48] [49]

To determine the parameters of the microstructures of each phase there is a number of methods that had been proposed, for example intercept method [50], XCT measurement method [51], pore and solid chord distributions [52], continuous phase size distribution (PSD_C) [53] and discrete phase size distribution (PSD_D) [54]. These different methods for calculating phase size all defines geometrical values of the object varyingly, thus they all result in different phase size distribution curves. It is important to choose the most suitable type of method for a certain type of application.

To calculate TPB length from a FIB-SEM image there need to be a methodical approach. However, it seems to be that there is no established method to estimate TPB length for a FIB-SEM model. The accuracy of evaluation greatly depends on different methods and process. One method that could predict TPB length is the volume expansion method [55]. In a 3D model, TPB is a line with the three volumes of phases in contact. If we try to expand the volume in each phase TPB will be like a tube and the centerlines of the tubes are the TPBs. For these theoretical lines to match TPB as closely as possible the resolution of the 3D model needs to be high and the volume expansion needs to be sufficiently small. Another way to calculate TPB length is by using voxels in the 3D image [56]. Each of the voxels is labeled as one of the three phases. One edge of the voxel will be in touch with four voxels and if the edge is shared by the three phases it is considered to be a TPB. This method also defines TPB to be of three states: active, inactive and unknown. Connectivity of the three states is traced across the 3D model. If the electronic and ionic state could be traced across the electrolyte to the outside or current collector, it is to be an active TPB. If the TPB is isolated it is an inactive TPB. If the TPB extends outside of the test region, it is an unknown TPB. The summation of the

total voxel edge that is active is the total TPB length. Similar method that predicts TPB length is the centroid method [57][29]. This method is similar to the prior method utilizing 3D model, but instead of using side length of the voxel it smooths it out using centroid of the TPB segments. The 3D model defines voxels with either electronic, ionic or gas phase. This method defines a voxel as the TPB if neighboring four voxels includes every three phases and the phase of diagonal voxels are not the same. The line surrounded by the four voxels is defined as the TPB segment. Next, three midpoints of the three neighboring triple phase boundary segment form a triangle. The centroid of these triangles is used to calculate triple phase boundary length.

These advanced TPB calculation techniques could give a better insight to the microstructure of the electrode. Spherical assumption may also not be practical for certain types of material. Using FIB-SEM allows for a more flexible way of calculating TPB length. This experimented data could be used to compare to theoretical calculations of TPB. This could give us a new way to modify mathematical calculations to precise the results.

In summary, for future research, the first step would be to reliably fabricate multi-wall CNT with homogeneous qualities. Second, fabricate YSZ-CNT composite with desired volume ratio. Third, examine microstructure with FIB-SEM equipment to create a 3D model. It is worth noting that currently there are no research that focus on using FIB-SEM to examine YSZ-CNT composite. Finally, analyze the 3D model through different methods to calculate TPB length. Typical fuel cell component testing could also be conducted such as impedance spectra, resistance, and ionic conductivity. These properties could be measured under different temperature to better understand the effect of temperature for YSZ-CNT composite. Voltage and power density function could be graphed as a function of current density if a single cell is ultimately fabricated. Ultimately,

if this new material were to be recognized as an improvement versus current SOFC technology, it could push SOFC further towards commercialization and benefit more applications.

References

[1] W. G. C. Ryan O'hayre, Suk-Won Cha, *Fuel Cell Fundamentals*. 2016.

[2] R. M. Ormerod, "Solid oxide fuel cells," *Chem. Soc. Rev.*, vol. 32, no. 1, pp. 17–28, 2003.

[3] Edited by P. J. Gellings & H.J .M. Bouwmeester, *The CRC Handbook of Solid State Electrochemistry*, vol. 7, no. 1. 1997.

[4] N. Q. Minh, "Solid oxide fuel cell technology - Features and applications," *Solid State Ionics*, vol. 174, no. 1–4. pp. 271–277, 2004.

[5] "The International Fuel Cells, a United Technology Company. Fuel Cells Review.," 2000.

[6] B. C. H. Steele and A. Heinzel, "Materials for fuel-cell technologies," *Nature*, vol. 414, no. 6861, pp. 345–352, Nov. 2001.

[7] E. D. Wachsman and K. T. Lee, "Lowering the temperature of solid oxide fuel cells," *Science*, vol. 334, no. 6058. pp. 935–939, 2011.

[8] J. W. Fergus, "Electrolytes for solid oxide fuel cells," *J. Power Sources*, vol. 162, no. 1, pp. 30–40, 2006.

[9] S. C. Singhal, "Solid oxide fuel cells," *Electrochem. Soc. Interface*, vol. 16, no. 4, pp. 41–44, 2007.

[10] A. B. Stambouli and E. Traversa, "Solid oxide fuel cells (SOFCs): A review of an environmentally clean and efficient source of energy," *Renew. Sustain. Energy Rev.*, vol. 6, no. 5, pp. 433–455, 2002.

[11] Á. Varga and S. Mounsey, "Fuel Cells," *University of Cambridge DoITPoMS*. .

[12] A. Mahajan, A. Kingon, Á. Kukovecz, Z. Konya, and P. M. Vilarinho, "Studies on the thermal decomposition of multiwall carbon nanotubes under different

atmospheres," *Mater. Lett.*, vol. 90, pp. 165–168, 2013.

[13] R. Pinedo *et al.*, "A straightforward synthesis of carbon nanotube–perovskite composites for solid oxide fuel cells," *J. Mater. Chem.*, vol. 21, no. 28, p. 10273, 2011.

[14] M. J. Santillán, A. Caneiro, F. C. Lovey, N. Quaranta, and A. R. Boccaccini, "Electrophoretic Codeposition of La<inf>0.6</inf>Sr<inf>0.4</inf>Co <inf>0.8</inf>Fe<inf>0.2</inf>O<inf>3-δ</inf> and carbon nanotubes for developing composite cathodes for intermediate temperature solid oxide fuel cells," *Int. J. Appl. Ceram. Technol.*, vol. 7, no. 1, 2010.

[15] K. Gong, F. Du, Z. Xia, M. Durstock, and L. Dai, "Nitrogen-doped carbon nanotube arrays with high electrocatalytic activity for oxygen reduction," *Science (80-.).*, vol. 323, no. 5915, pp. 760–764, 2009.

[16] S. Wang, D. Yu, and L. Dai, "Polyelectrolyte functionalized carbon nanotubes as efficient metal-free electrocatalysts for oxygen reduction," *J. Am. Chem. Soc.*, vol. 133, no. 14, pp. 5182–5185, 2011.

[17] V. . Kharton and F. M. . Marques, "Mixed ionic–electronic conductors: effects of ceramic microstructure on transport properties," *Curr. Opin. Solid State Mater. Sci.*, vol. 6, no. 3, pp. 261–269, Jun. 2002.

[18] H. Rickert, *Electrochemistry of Solids*. Berlin: Springer, 1982.

[19] I. Riess, "Mixed ionic–electronic conductors—material properties and applications," *Solid State Ionics*, vol. 157, no. 1–4, pp. 1–17, Feb. 2003.

[20] J. Van Herle and a. J. McEvoy, "Oxygen diffusion through silver cathodes for solid oxide fuel cells," *J. Phys. Chem. Solids*, vol. 55, no. 4, pp. 339–347, 1994.

[21] N. Q. Minh and T. Takahshi, "Science and Technology of Ceramic Fuel Cells," *Comp. Educ.*, vol. 49, no. March, pp. 374–387, 2013.

[22] P. J. G. H. J. M. Bouwmeester, *Handbook of Solid State Electrochemistry*. CRC Press, 1997.

[23] H. A. Taroco, J. A. F. Santos, R. Z. Domingues, and T. Matencio, *Advances in Ceramics*. 2011.

[24] F. Lamarche and C. Leroy, “Evaluation of the volume of intersection of a sphere with a cylinder by elliptic integrals,” *Comput. Phys. Commun.*, vol. 59, no. 2, pp. 359–369, 1990.

[25] “Game Development Stack Exchange Sphere-Sphere intersection and Circle-Sphere intersection.” .

[26] W. F. Kern and J. R. Bland, *Solid Mensuration with Proofs, 2nd ed.* Wiley, 1948.

[27] J. R. Wilson *et al.*, “Three dimensional reconstruction of solid oxide fuel cell electrodes using focused ion beam - Scanning electron microscopy,” *ECS Trans.*, vol. 7, no. 1 PART 2, pp. 1879–1887, 2007.

[28] M. Kishimoto, H. Iwai, M. Saito, and H. Yoshida, “Quantitative evaluation of solid oxide fuel cell porous anode microstructure based on focused ion beam and scanning electron microscope technique and prediction of anode overpotentials,” *J. Power Sources*, vol. 196, no. 10, pp. 4555–4563, 2011.

[29] N. Shikazono, D. Kanno, K. Matsuzaki, H. Teshima, S. Sumino, and N. Kasagi, “Numerical Assessment of SOFC Anode Polarization Based on Three-Dimensional Model Microstructure Reconstructed from FIB-SEM Images,” *J. Electrochem. Soc.*, vol. 157, no. 5, p. B665, 2010.

[30] M. Brown, S. Primdahl, and M. Mogensen, “Structure/Performance Relations for Ni/Yttria-Stabilized Zirconia Anodes for Solid Oxide Fuel Cells,” *J. Electrochem. Soc.*, vol. 147, no. 2, pp. 475–485, 2000.

[31] J. H. Lee, H. Moon, H. W. Lee, J. Kim, J. D. Kim, and K. H. Yoon, “Quantitative

analysis of microstructure and its related electrical property of SOFC anode, Ni-YSZ cermet," *Solid State Ionics*, vol. 148, no. 1–2, pp. 15–26, 2002.

[32] M. Han, X. Tang, H. Yin, and S. Peng, "Fabrication, microstructure and properties of a YSZ electrolyte for SOFCs," *J. Power Sources*, vol. 165, no. 2, pp. 757–763, 2007.

[33] X. Wang *et al.*, "Size-controlled large-diameter and few-walled carbon nanotube catalysts for oxygen reduction," *Nanoscale*, vol. 7, no. 47, pp. 20290–20298, 2015.

[34] G. Moskal, "Characteristics of selected thermal properties of 8YSZ type powders produced with different methods," *IOP Conf. Ser. Mater. Sci. Eng.*, vol. 15, p. 12065, Nov. 2010.

[35] P. K. Sekhar, E. L. Brosha, R. Mukundan, M. A. Nelson, D. Toracco, and F. H. Garzon, "Effect of yttria-stabilized zirconia sintering temperature on mixed potential sensor performance," *Solid State Ionics*, vol. 181, no. 19–20, pp. 947–953, 2010.

[36] L. Zhang, S. P. Jiang, W. Wang, and Y. Zhang, "NiO/YSZ, anode-supported, thin-electrolyte, solid oxide fuel cells fabricated by gel casting," *J. Power Sources*, vol. 170, no. 1, pp. 55–60, Jun. 2007.

[37] S. D. Kim, H. Moon, S. H. Hyun, J. Moon, J. Kim, and H. W. Lee, "Ni-YSZ cermet anode fabricated from NiO-YSZ composite powder for high-performance and durability of solid oxide fuel cells," *Solid State Ionics*, vol. 178, no. 21–22, pp. 1304–1309, 2007.

[38] S. Zha, Y. Zhang, and M. Liu, "Functionally graded cathodes fabricated by sol-gel/slurry coating for honeycomb SOFCs," *Solid State Ionics*, vol. 176, no. 1–2, pp. 25–31, 2005.

[39] G. Li, Z. Sun, H. Zhao, C. Chen, and R. Ren, “Effect of temperature on the porosity, microstructure, and properties of porous La0.8Sr0.2MnO3 cathode materials,” *Ceram. Int.*, vol. 33, no. 8, pp. 1503–1507, 2007.

[40] H. A. Hamedani, K. H. Dahmen, D. Li, H. Peydaye-Saheli, H. Garmestani, and M. Khaleel, “Fabrication of gradient porous LSM cathode by optimizing deposition parameters in ultrasonic spray pyrolysis,” *Mater. Sci. Eng. B Solid-State Mater. Adv. Technol.*, vol. 153, no. 1–3, pp. 1–9, 2008.

[41] J. J. Choi *et al.*, “Low temperature fabrication of nano-structured porous LSM-YSZ composite cathode film by aerosol deposition,” *J. Alloys Compd.*, vol. 509, no. 5, pp. 2627–2630, 2011.

[42] R. Chaim, M. Levin, A. Shlayer, and C. Estournes, “Sintering and densification of nanocrystalline ceramic oxide powders: a review,” *Adv. Appl. Ceram.*, vol. 107, no. 3, pp. 159–169, 2008.

[43] Z. H. Zhang, Z. F. Liu, J. F. Lu, X. B. Shen, F. C. Wang, and Y. D. Wang, “The sintering mechanism in spark plasma sintering - Proof of the occurrence of spark discharge,” *Scr. Mater.*, vol. 81, pp. 56–59, 2014.

[44] R. Chaim, A. Shlayer, and C. Estournes, “Densification of nanocrystalline Y2O3 ceramic powder by spark plasma sintering,” *J. Eur. Ceram. Soc.*, vol. 29, no. 1, pp. 91–98, 2009.

[45] M. Mazaheri, D. Mari, R. Schaller, G. Bonnefont, and G. Fantozzi, “Processing of yttria stabilized zirconia reinforced with multi-walled carbon nanotubes with attractive mechanical properties,” *J. Eur. Ceram. Soc.*, vol. 31, no. 14, pp. 2691–2698, 2011.

[46] A. Karanam, L. Bichler, and R. Fong, “On the Densification Behavior of (0.2, 0.5, and 1 Wt Pct) CNT-YSZ Ceramic Composites Processed via Spark Plasma

Sintering," *Metall. Mater. Trans. B Process Metall. Mater. Process. Sci.*, vol. 46, no. 4, pp. 1666–1673, 2015.

[47] A. Duszová, J. Dusza, K. Tomášek, G. Blugan, and J. Kuebler, "Microstructure and properties of carbon nanotube/zirconia composite," *J. Eur. Ceram. Soc.*, vol. 28, no. 5, pp. 1023–1027, 2008.

[48] L. Holzer, B. Münch, B. Iwanschitz, M. Cantoni, T. Hocker, and T. Graule, "Quantitative relationships between composition, particle size, triple phase boundary length and surface area in nickel-cermet anodes for Solid Oxide Fuel Cells," *J. Power Sources*, vol. 196, no. 17, pp. 7076–7089, Sep. 2011.

[49] L. Holzer *et al.*, "Microstructure degradation of cermet anodes for solid oxide fuel cells: Quantification of nickel grain growth in dry and in humid atmospheres," *J. Power Sources*, vol. 196, no. 3, pp. 1279–1294, 2011.

[50] A. Faes, A. Hessler-Wyser, D. Presvytes, C. G. Vayenas, and J. Vanherle, "Nickel-zirconia anode degradation and triple phase boundary quantification from microstructural analysis," *Fuel Cells*, vol. 9, no. 6, pp. 841–851, 2009.

[51] K. N. Grew *et al.*, "Nondestructive Nanoscale 3D Elemental Mapping and Analysis of a Solid Oxide Fuel Cell Anode," *J. Electrochem. Soc.*, vol. 157, no. 6, p. B783, 2010.

[52] I. Cousin, P. Levitz, and A. Bruand, "Three-dimensional analysis of a loamy-clay soil using pore and solid chord distributions," *Eur. J. Soil Sci.*, vol. 47, no. 4, pp. 439–452, 1996.

[53] B. Münch and L. Holzer, "Contradicting geometrical concepts in pore size analysis attained with electron microscopy and mercury intrusion," *J. Am. Ceram. Soc.*, vol. 91, no. 12, pp. 4059–4067, 2008.

[54] B. Münch, P. Gasser, L. Holzer, and R. Flatt, "FIB-nanotomography of particulate

systems - Part II: Particle recognition and effect of boundary truncation," *J. Am. Ceram. Soc.*, vol. 89, no. 8, pp. 2586–2595, 2006.

[55] H. Iwai *et al.*, "Quantification of SOFC anode microstructure based on dual beam FIB-SEM technique," *J. Power Sources*, vol. 195, no. 4, pp. 955–961, 2010.

[56] K. T. Lee, N. J. Vito, and E. D. Wachsman, "Comprehensive quantification of Ni–Gd0.1Ce0.9O1.95 anode functional layer microstructures by three-dimensional reconstruction using a FIB/SEM dual beam system," *J. Power Sources*, vol. 228, pp. 220–228, Apr. 2013.

[57] H. Iwai *et al.*, "Quantification of SOFC anode microstructure based on dual beam FIB-SEM technique," *J. Power Sources*, vol. 195, no. 4, pp. 955–961, Feb. 2010.

Biographical Information

Shiuan-Duo Chaing was born in Taipei, Taiwan. He received his bachelor's degree in Mechanical Engineering from National Central University, Taoyuan Taiwan in July 2016. He started M.S. in Mechanical engineering from The University of Texas at Arlington in Fall 2016.

He started working under Dr. Leila Ladani's supervision on May 2017. His research mainly includes solid oxide fuel cells and triple phase boundary calculations. Other research also includes microfabrication process and fabrication of CNT.